

ChemComm

Accepted Manuscript



This is an *Accepted Manuscript*, which has been through the Royal Society of Chemistry peer review process and has been accepted for publication.

Accepted Manuscripts are published online shortly after acceptance, before technical editing, formatting and proof reading. Using this free service, authors can make their results available to the community, in citable form, before we publish the edited article. We will replace this *Accepted Manuscript* with the edited and formatted *Advance Article* as soon as it is available.

You can find more information about *Accepted Manuscripts* in the [Information for Authors](#).

Please note that technical editing may introduce minor changes to the text and/or graphics, which may alter content. The journal's standard [Terms & Conditions](#) and the [Ethical guidelines](#) still apply. In no event shall the Royal Society of Chemistry be held responsible for any errors or omissions in this *Accepted Manuscript* or any consequences arising from the use of any information it contains.

COMMUNICATION

Hybrid with Uniaxial Negative Thermal Expansion Behaviour: Synergistic Role of Organic and Inorganic Components

Cite this: DOI: 10.1039/x0xx00000x

Received 00th January 2012,
Accepted 00th January 2012

DOI: 10.1039/x0xx00000x

www.rsc.org/

Kai-Yao Wang,^a Mei-Ling Feng,^a Liu-Jiang Zhou,^a Jian-Rong Li,^a Xing-Hui Qi^{a,b}
and Xiao-Ying Huang^{*,a}

Presented is an inorganic-organic hybrid compound $\text{Mn}_2(\text{api})\text{Sb}_2\text{S}_5$ (**1**) with uniaxial NTE behaviour. The NTE of **1** reflects a strong synergistic role of organic and inorganic components, which results from the novel zigzag linkage of interlamellar organic ligands. An “elevator-platform” expansion mechanism was proposed, with implications for future design of sensitive hybrid thermomechanical actuators.

Most crystalline materials on heating experience modest positive thermal expansion (PTE) along all three crystallographic axes due to an increasing anharmonic vibrations of the constituent atoms, molecules or ions. In rare cases, specific structural features may result in the contraction or insensitivity of the volume or length upon heating, that is, the negative thermal expansion (NTE).¹ Extensive studies in various materials e.g. oxides, metal cyanides and metal-organic frameworks (MOFs) confirmed the important structure-function relationships hidden behind this special behaviour.² Thus, it is undoubtedly interesting to study the thermal expansion behaviour of materials with novel structural features, which may help to explore new mechanism or even design functional materials with desirable properties.

Crystalline hybrids with periodically ordered arrangement of organic molecules and inorganic motifs at atomic level have emerged as a new class of materials that are of fundamental significance and potential applications.³ One milestone is the development of three-dimensional (3D) II-VI based hybrid semiconductors with a general formula of $[\text{MQ}(\text{L})_6]_n$ ($\text{M} = \text{Mn}, \text{Zn}, \text{Cd}$; $\text{Q} = \text{S}, \text{Se}, \text{Te}$; $\text{L} = \text{diamine}$).⁴ Their structures comprise of alternating assemblies of MQ layers and diamine molecules that interconnect the layers via coordination bonds. Studies reveal that the inorganic layers and acyclic amines in such blended system might display distinct PTE and NTE along the direction perpendicular to the layers, whose combination endows the hybrid lattice absorbing uniaxial zero thermal expansion (ZTE) capacity.⁵ These studies highlight the important influence of

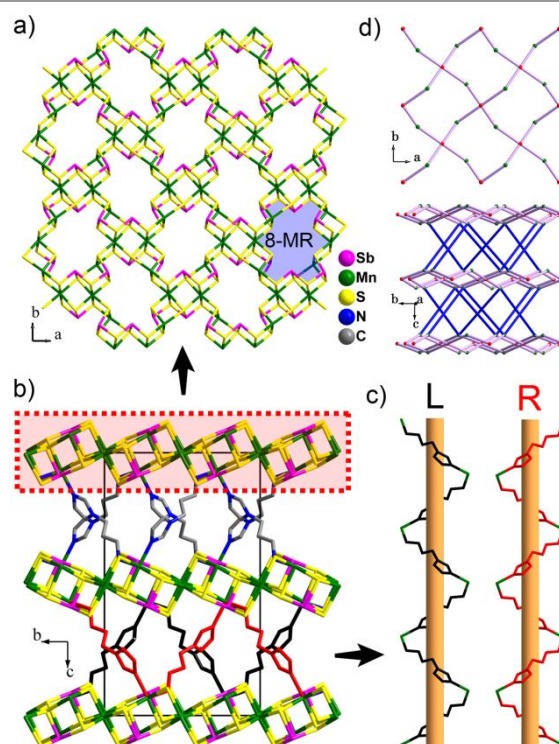


Fig. 1 Structures of (a) the $\{ \text{Mn}_2\text{Sb}_2\text{S}_5 \}_n$ layer and (b) the 3D-hybrid framework of **1**. (c) The left- and right-handed helical chains running along the *b* axis. (d) Topologies of the $\{ \text{Mn}_2\text{Sb}_2\text{S}_5 \}_n$ layer (top) and the $(6^2.8^3)(6^4.8^2)_2$ net in the structure of **1** (bottom). The red/green nodes represent $\{ \text{Mn}_2\text{Sb}_2\text{S}_5 \}$ / $\{ \text{MnSbS}_2 \}$ cores.

arrangement of inorganic and organic segments on the physical properties. Herein, we developed a new strategy to design hybrid materials with uniaxial NTE property. The strategy is demonstrated by an unprecedented 3D organic-inorganic hybrid compound, namely, $\text{Mn}_2(\text{api})\text{Sb}_2\text{S}_5$ ($\text{api} = \text{N}$ -(3-aminopropyl)-imidazole (**1**), Fig. 1.

Different from the parallel arrangement in $[MQ(L)_{0.5}]_n$, the interlamellar organic species of **1** adopt a staggered arrangement mode which enables the presence of an angle between adjacent ligands. This angle correlates positively to the PTE of inorganic layer on the plane. Furthermore, such angular correlation can incorporate the NTE of organic ligand itself to form a remarkable enhanced uniaxial NTE perpendicular to the inorganic layers in the whole lattice. Correspondingly, we put forward a novel "elevator-platform" expansion mechanism to explain the NTE behaviour of **1**.

1 was synthesized through a solvothermal reaction of elemental Mn, Sb, and S in a mixture of api and $N_2H_4 \cdot H_2O$, where the api acted as both organic ligand and solvent, Scheme S1. Comparison of the reactions with different amount of S powder gave the best molar ratio of Mn: Sb: S = 1: 1: 6, indicating the necessity of an excess of the S source for the synthesis.⁶ Further detailed synthetic experiments illustrated that the addition of an appropriate, small amount of $N_2H_4 \cdot H_2O$ with the optimal volume ratio of $N_2H_4 \cdot H_2O$: api of 1: 15 could largely enhance the crystal dimension and quality to a level that was suitable for single crystal X-ray diffraction. The $N_2H_4 \cdot H_2O$ did not enter the final structure of **1**, but it might play an important role of auxiliary agent, according to the literatures.⁷

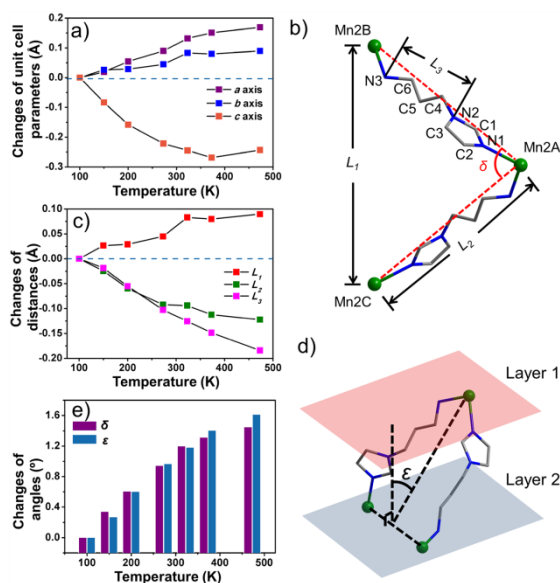


Fig. 2 (a) Changes of unit cell parameters of **1** as a function of temperature. (b) Representation of L_1 , L_2 , L_3 and δ . (c) Changes of L_1 , L_2 , L_3 as a function of temperature. (d) Representation of ϵ between adjacent $\{Mn_2Sb_2S_3\}_n$ layers. (e) Changes of δ and ϵ as a function of temperature.

Compound **1** crystallizes in the orthorhombic space group $Pbca$, consisting of $\{Mn_2Sb_2S_3\}_n$ layers⁸ interlinked by the api ligands via Mn–N coordination bonds. The asymmetric unit contains two Mn^{2+} ions, two Sb^{3+} ions, five S^{2-} ions, and one api molecule, Fig. S1. Both Sb^{3+} ions are coordinated by three S^{2-} ions. Nevertheless, the two Mn^{2+} ions have different coordination environments. The Mn1 is octahedrally surrounded by six S^{2-} ions, while the Mn2 is coordinated by four S^{2-} ions and two N atoms in *cis*-configuration. Two Sb1 and two Mn1 are connected by six μ_3 - S^{2-} ions to form a di-semi-cubane-like $\{Mn_2Sb_2S_3\}$ core, while one Sb2 and one Mn2 couple into a $\{MnSbS_3\}$ core with a common-shared S_3 – S_4 edge. Alternating interlinkages of $\{Mn_2Sb_2S_3\}$

cores and $\{MnSbS_3\}$ cores in a 1:2 ratio give rise to a honeycomb-like $\{Mn_2Sb_2S_3\}_n$ layer, with concomitant formation of a 8-membered ring (8-MR) of $\{Mn_4Sb_4S_8\}$, Fig. 1a. The layers stack in an *ABAB* sequence along the *c* axis. The organic api linkers weave the inorganic layers into a final 3D framework by connecting Mn2 ions from adjacent layers, Fig. 1b. Meanwhile, the api ligands are interlinked end to end by the Mn2 joints to form a zigzag helical chain running along the a_1 axis parallel to the *b* axis, where both left- and right-handed chirality are founded as a result of centrosymmetric nature of the structure, Fig. 1c. Both helixes have a pitch of 12.2724(7) Å (100K). From the topological viewpoint, the 3D framework of **1** has a topology of $(6^2.8^4)(6^4.8^2)_2$ built upon a 4,4-connected net, in which both the $\{Mn_2Sb_2S_3\}$ and $\{MnSbS_3\}$ cores act as 4-connected nodes, Fig. 1d.

T (K)	TT%/TG%	Conformations of The Chain
100	–	
150	–	
200	87.9 : 12.1	
273	77.9 : 22.1	
323	75.9 : 24.1	
373	70.9 : 29.1	
473	63.3 : 36.7	

Fig. 3 The TT%:TG% of the N2–C4–C5–C6–N3 chain in **1** in different temperatures and their conformations.

Dark yellow crystals of **1** is thermally stable up to 300 °C and is stable in air for more than one year, which is preferable for tracking its thermal behaviour. Variable-temperature single crystal X-ray diffractions (SC-XRD) were performed on the same crystal at 100, 150, 200, 273, 323, 373 and 473 K, where the corresponding structural codes are abbreviated as **1-100K**, **1-150K**, **1-200K**, **1-273K**, **1-323K**, **1-373K** and **1-473K**. The unit cell parameters *a*, *b* and *c* in different temperatures are listed in Table S3. Fig. 2a shows the changes of the unit cell parameters of **1**. Clearly, the *a* and *b* axes that are parallel to the $\{Mn_2Sb_2S_3\}_n$ layer respond positively to the increase of the temperature, with their thermal expansion coefficients of $36.4 \times 10^{-6} K^{-1}$ (α_a) and $19.6 \times 10^{-6} K^{-1}$ (α_b) (100–473 K), respectively, suggesting a typical PTE behaviour of the layer in expansion directions. In contrast, the *c* axis perpendicular to the $\{Mn_2Sb_2S_3\}_n$ layer shows an obvious NTE phenomenon. The thermal expansion coefficient in *c* direction kept a maximum $\alpha_{c,max}$ of $-75.0 \times 10^{-6} K^{-1}$ in the temperature range 100–200 K and began to decrease gradually when the temperature rose up to 200 K, resulting in an average α_c (100–373 K) value of $-46.7 \times 10^{-6} K^{-1}$, larger than the isotropic material ZrW_2O_8 ($\alpha_a = -9.1 \times 10^{-6} K^{-1}$) and $Cd(CN)_2$ ($\alpha_a = -20 \times 10^{-6} K^{-1}$).^{2a,2d} The rebound of the length of *c* axis in 473K is due to the increasing thickness of the $\{Mn_2Sb_2S_3\}_n$ layer, Fig. S2 and Table S4. Such kind of uniaxial NTE is still very limited nowadays, where the current records of "colossal" values are held by the $Ag_3[Co(CN)_6]$ ($\alpha_c = -130 \times 10^{-6} K^{-1}$)⁹ and FMOF-1 ($\alpha_c = -170 \times 10^{-6} K^{-1}$).¹⁰ In comparison, the $\alpha_{c,max}$ of **1** has been around half of these "colossal" ones, laying in a considerable magnitude. More importantly, this finding provides the first example to prospect the development of inorganic-organic hybrids in the uniaxial NTE study.

It is possible to rationalize the mechanism of the uniaxial NTE at the atomic level. Here, three Mn₂ ions (Mn₂A belongs to layer 1; Mn₂B, Mn₂C belong to layer 2) connected by two api ligands were taken as a model, where the distances of Mn₂B...Mn₂C, Mn₂A...Mn₂B/Mn₂C and N₂...N₃ are denoted as L_1 , L_2 and L_3 , Fig. 2b. L_1 responds positively as a function of temperature on account of its equal length as parameter b , Fig. 2c. In contrast, L_2 and L_3 contract from 10.9660(6) and 4.9919(35) Å at 100K to 10.8433(15) and 4.8096(88) Å at 473K, resulting in the $\Delta L_2/L_2$ and $\Delta L_3/L_3$ as large as -1.1% and -3.7% in this temperature range. These changes may attribute to the NTE behaviour of the acyclic amines caused by the partial conformation transfer of the N₂-C₄-C₅-C₆-N₃ chain in **1**, Fig. 3. At 100 and 150 K, the two C-C bonds in this chain are both *trans* (*T*), namely *TT*. However, according to the refinement results, a disorder phenomenon occurs to the C₄, C₅, C₆ atoms at 200, 273, 323, 373, and 473 K. The torsion angles of the C₄-C₅-C₆-N₃ and C₄B-C₅B-C₆B-N₃ chains turn out to be -180 and -60°, illustrating a partial transition of the C₅-C₆ bond to *gauche* (*G*), leading to a *TG* conformation. The detected proportion of *TG* are 12.1% (200K), 22.1% (273K), 24.1% (323K), 29.1% (373K) and 36.7% (473K), roughly showing an aggravation with the increase of temperature. As a result, this conformation transition assists the contraction of L_3 , resulting in an overall decreasing L_2 . The values of L_1 , L_2 , L_3 and ratio of *TT* : *TG* % are listed in Table S3 and Fig. 3. In addition, we define the angle between Mn₂B...Mn₂A...Mn₂C as δ , and the angle between the plane going through Mn₂A, Mn₂B, Mn₂C and the normal to the {Mn₂Sb₂S₃}_n plane as ϵ , Figs. 2b and d. The values of δ and ϵ in different temperatures are listed in Table S3. From 100 to 473 K, the enlargement of L_1 and contraction of L_2 contribute to an increase of 1.452(14)° on the δ degree, Fig. 2e. Simultaneously, the ϵ degree also increases by 1.613(10)° due to the expansion of the {Mn₂Sb₂S₃}_n in the *a* direction, together with contraction of L_2 , Fig. 2e. These two angular changes are conducive to the contraction of *c*-axis, according to the arranging mode of ligands in the structure of **1**. The vital role of the tilted stacking of organic species on the anisotropic property resembles the case of (*S,S*)-octa-3,5-diyne-2,7-diol, where the molecules adjust their orientations as a function of temperature to maintain an efficient packing, with concomitant large NTE perpendicular to the packing direction.¹¹

From the geometrical flexibility viewpoint, a garden lattice fencing-like mechanism can briefly reflect the role of biaxial PTE of the {Mn₂Sb₂S₃}_n layer on the overall NTE of **1**.^{9,12} However, a further concern about the NTE of the organic ligand itself should also be highlighted in such a blended hybrid system. Therefore, to emphasize the synergistic effect, we attribute the mechanism for the uniaxial NTE of **1** to a new temperature-controlled "elevator-platform" that stretches along the *c* axis, Fig. 4. The abstraction of the structure of **1** gives a pillared-layer framework, where the flexible aminopropyl group of the api molecular pillar and the inorganic {Mn₂Sb₂S₃}_n layer can be viewed as NTE spring and PTE network, respectively. When temperature goes up, the N₂...N₃ spring displays a contraction ($\Delta L_3 < 0$). The expansion of the network in the plane results in $\Delta\delta > 0$, as well as $\Delta\epsilon > 0$ (for clarity, ϵ is not represented in Fig. 4). All three changes play harmonic roles on the decrease of the distance between two adjacent networks ($\Delta d < 0$, d is equal to half the unit cell parameter *c*). When the temperature goes down, the case turns out to be opposite.

This "elevator-platform" mechanism provides a strategy to synthesize uniaxial NTE hybrid materials, that is, to build up the synergistic combination of NTE of organic ligand and angular changes between adjacent ligands caused by the PTE of inorganic layer on the plane through a staggered linkage of interlamellar organic ligands. Three significant aspects are concerned in choosing the inorganic and organic motifs: (a) the inorganic layer displays an obvious PTE performance on the plane; (b) in the inorganic layer, there are M^{n+} ions containing two vacant coordination sites which can act as linking nodes for the staggered arrangement of organic ligands; (c) a polar, bidentate ligand consisting of acyclic chain and rigid group is preferred to maintain the NTE character, simultaneously avoiding the chelation on the same M^{n+} ion.

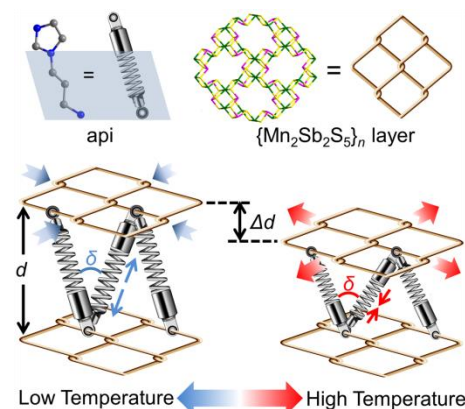


Fig. 4 Structures of the api ligand (top left) and {Mn₂Sb₂S₃}_n layer (top right) and their simplified abstractions and representation of the synergistic role of organic and inorganic components on the uniaxial NTE in **1** (bottom).

In summary, we present here a unique strategy to design hybrids with uniaxial NTE. It is revealed that the specific zigzag linkage of interlamellar organic ligands is the key to build up the synergistic combination of NTE of organic ligand due to the partial conformation transfer and angular changes between adjacent ligands caused by the PTE of inorganic layer on the plane. We put forward a novel concept of "elevator-platform" expansion mechanism. The finding further highlights the arrangement of inorganic and organic segments on the physical properties, with implications for future design of sensitive thermomechanical actuators.

This work was supported by grants from the NNSF of China (Nos. 21221001 and 21171164) and the 973 program (No. 2012CB821702).

Notes and references

^a State Key Laboratory of Structural Chemistry, Fujian Institute of Research on the Structure of Matter, the Chinese Academy of Sciences, Fuzhou, Fujian 350002, P.R. China. E-mail: xyhuang@fjirsm.ac.cn; Fax: +86 591-83793727; Tel: +86-591 83793727.

^b College of Chemistry, Fuzhou University, Fuzhou, Fujian 350002, P.R. China

† Electronic Supplementary Information (ESI) available: experimental details, crystallographic data, PXRD patterns, DFT calculations, and magnetic analysis. See DOI: 10.1039/c000000x/ CCDC numbers 1008730-1008736 for **1-100K**, **1-150K**, **1-200K**, **1-273K**, **1-323K**, **1-373K** and **1-473K**.

- 1 (a) A. W. Sleight, *Annu. Rev. Mater. Sci.*, 1998, **28**, 29-43; (b) W. Miller, C. W. Smith, D. S. Mackenzie, K. E. Evans, *J. Mater. Sci.*, 2009, **44**, 5441-5451.
- 2 (a) T. A. Mary, J. S. O. Evans, T. Vogt, A. W. Sleight, *Science*, 1996, **272**, 90-92; (b) J. S. O. Evans, Z. Hu, J. D. Jorgensen, D. N. Argyriou, S. Short, A. W. Sleight, *Science*, 1997, **275**, 61-65; (c) K. W. Chapman, P. J. Chupas, C. J. Kepert, *J. Am. Chem. Soc.*, 2005, **127**, 15630-15636; (d) A. L. Goodwin, C. J. Kepert, *Phys. Rev. B*, 2005, **71**, 140301; (e) K. W. Chapman, P. J. Chupas, C. J. Kepert, *J. Am. Chem. Soc.*, 2006, **128**, 7009-7014; (f) A. E. Phillips, A. L. Goodwin, G. J. Halder, P. D. Southon, C. J. Kepert, *Angew. Chem. Int. Ed.*, 2008, **47**, 1396-1399; (g) V. K. Peterson, G. J. Kearley, Y. Wu, A. J. Ramirez-Cuesta, E. Kemner, C. J. Kepert, *Angew. Chem. Int. Ed.*, 2010, **49**, 585-588; (h) N. Lock, M. Christensen, C. J. Kepert, B. B. Iversen, *Chem. Commun.*, 2013, **49**, 789-791; (i) Y. Wu, V. K. Peterson, E. Luks, T. A. Darwish, C. J. Kepert, *Angew. Chem. Int. Ed.*, 2014, **53**, 5175-5178; (j) I. E. Collings, M. G. Tucker, D. A. Keen, A. L. Goodwin, *CrystEngComm*, 2014, **16**, 3498-3506.
- 3 (a) P. J. Hagrman, D. Hagrman, J. Zubieta, *Angew. Chem. Int. Ed.*, 1999, **38**, 2638-2684; (b) C. Sanchez, B. Julián, P. Belleville, M. Popall, *J. Mater. Chem.*, 2005, **15**, 3559-3592; (c) H.-B. Yao, M.-R. Gao, S.-H. Yu, *Nanoscale*, 2010, **2**, 322-334.
- 4 (a) X. Huang, J. Li, H. Fu, *J. Am. Chem. Soc.*, 2000, **122**, 8789-8790; (b) X. Huang, H. R. Heulings IV, V. Le, J. Li, *Chem. Mater.*, 2001, **13**, 3754-3759; (c) X. Huang, J. Li, Y. Zhang, A. Mascarenhas, *J. Am. Chem. Soc.*, 2003, **125**, 7049-7055.
- 5 (a) J. Li, W. Bi, W. Ki, X. Huang, S. Reddy, *J. Am. Chem. Soc.*, 2007, **129**, 14140-14141; (b) Y. Zhang, Z. Islam, Y. Ren, P. A. Parilla, S. P. Ahrenkiel, P. L. Lee, A. Mascarenhas, M. J. McNevin, I. Naumov, H.-X. Fu, X.-Y. Huang, J. Li, *Phys. Rev. Lett.*, 2007, **99**, 215901; (c) X. Zhang, Y. Ren, M. Roushan, J. Li, *Eur. J. Inorg. Chem.*, 2012, 5966-5971.
- 6 B. Seidlhofer, N. Pienack, W. Bensch, *Z. Naturforsch.*, 2010, **65b**, 937-975.
- 7 (a) J.-R. Li, Z.-L. Xie, X.-W. He, L.-H. Li, X.-Y. Huang, *Angew. Chem. Int. Ed.*, 2011, **50**, 11395-11399; (b) Y. Lin, D. Xie, W. Massa, L. Mayrhofer, S. Lippert, B. Ewers, A. Chernikov, M. Koch, S. Dehnen, *Chem. Eur. J.*, 2013, **19**, 8806-8813; (c) K.-Y. Wang, M.-L. Feng, D.-N. Kong, S.-J. Liang, L. Wu, X.-Y. Huang, *CrystEngComm* 2012, **14**, 90-94.
- 8 (a) W. Bensch, M. Schur, *Eur. J. Solid State Inorg. Chem.*, 1996, **33**, 1149-1160; (b) M. Schur, C. Näher, W. Bensch, *Z. Naturforsch.*, 2001, **56b**, 79-84; (c) M. Schur, W. Bensch, *Z. Naturforsch.*, 2002, **57b**, 1-7; (d) L. Engelke, R. Stähler, M. Schur, C. Näher, W. Bensch, R. Pötgen, M. H. Möller, *Z. Naturforsch.*, 2004, **59b**, 869-876; (e) A. Puls, C. Näher, W. Bensch, *Z. Anorg. Allg. Chem.*, 2006, **632**, 1239-1243; (f) X. Wang, T.-L. Sheng, S.-M. Hu, R.-B. Fu, X.-T. Wu, *Inorg. Chem. Commun.*, 2009, **12**, 399-401.
- 9 A. L. Goodwin, M. Calleja, M. J. Conterio, M. T. Dove, J. S. O. Evans, D. A. Keen, L. Peters, M. G. Tucker, *Science*, 2008, **319**, 794-797.
- 10 C. Yang, X. Wang, M. A. Omary, *Angew. Chem. Int. Ed.*, 2009, **48**, 2500-2505.
- 11 D. Das, T. Jacobs, L. J. Barbour, *Nat. Mater.*, 2010, **9**, 36-39.
- 12 A. B. Cairns, A. L. Thompson, M. G. Tucker, J. Haines, A. L. Goodwin, *J. Am. Chem. Soc.*, 2012, **134**, 4454-4456.

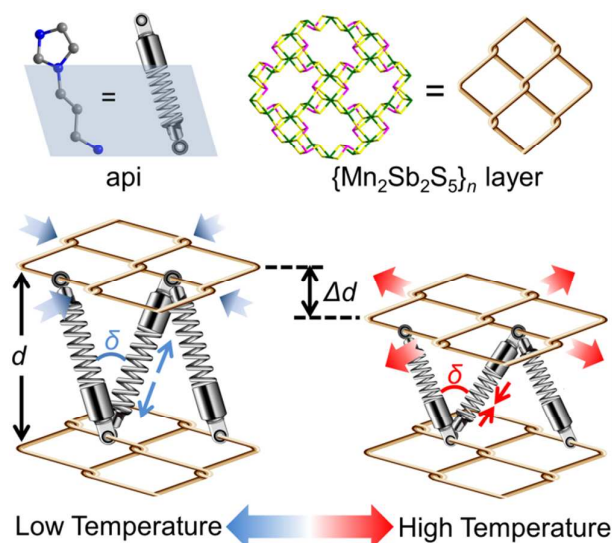
Table of Contents for

**Hybrid with Uniaxial Negative Thermal Expansion Behavior:
Synergistic Role of Organic and Inorganic Components**

Kai-Yao Wang,^a Mei-Ling Feng,^a Liu-Jiang Zhou,^a Jian-Rong Li,^a Xing-Hui Qi^{a,b} and
Xiao-Ying Huang^{*,a}

^a State Key Laboratory of Structural Chemistry, Fujian Institute of Research on the Structure of Matter, the Chinese Academy of Sciences, Fuzhou, Fujian 350002, P.R. China. E-mail: xyhuang@fjirsm.ac.cn; Fax: +86 591-83793727; Tel: +86-591 83793727.

^b College of Chemistry, Fuzhou University, Fuzhou, Fujian 350002, P.R. China



Through the study on a new $\text{Mn}_2(\text{api})\text{Sb}_2\text{S}_5$ compound, we propose a strategy for designing novel hybrid with uniaxial NTE behavior based on the synergistic role of organic and inorganic components.